nature structural & molecular biology

Cell-cycle coordination between DNA replication and recombination revealed by a vertebrate N-end rule degron-Rad51

Xinyi Su, Juan A Bernal & Ashok R Venkitaraman

Coordination of homologous DNA recombination (HDR) with DNA replication maintains the fidelity of cell division. Exploiting Varshavsky's N-end rule to create a thermosensitive degron for conditional genetics in an avian cell line, we confirm that inactivation of the essential HDR enzyme Rad51 in a single cell cycle does not stop replicative DNA synthesis but, instead, causes G2 arrest. Rad51 complementation after the completion of replication overcomes this block, suggesting that HDR becomes necessary in G2. Indeed, DNA structures that bind activated replication protein A accumulate during the S phase, to be preferentially resolved during G2 by a Rad51-dependent mechanism. Breaks affecting a single chromatid predominate after the first cell cycle without Rad51, subsequently evolving into isochromatid lesions. We suggest a model for the vertebrate cell cycle in which HDR during the G2 phase is separated from DNA replication in S phase and chromosome segregation in M.

Two of the key DNA transactions that underlie vertebrate cell division are compartmentalized into distinct phases of the cell cycle. Replicative DNA synthesis occurs in the S phase, and its completion is followed during the mitotic M phase by the condensation of duplicated chromosomal DNA and the segregation of chromosomes to daughter cells. A third DNA transaction, HDR, is also vital for the fidelity of the cell-division cycle[1–3], but it remains unclear when and how it may act.

In yeast and vertebrate cells, HDR begins when the DNA recombinase Rad51 oligomerizes on single-stranded DNA (ssDNA) substrates to form an ordered nucleoprotein filament that catalyzes invasion into duplex DNA and the pairing of homologous DNA strands, enabling strand exchange[4,5]. *In vitro* or *in vivo*, Rad51 is essential for the earliest steps in HDR and is assisted or regulated in this function by numerous accessory proteins[6,7]. In vertebrate cells, these include the Rad51 paralogs Rad51B, Rad51C, Xrcc3 or Rad51D, as well as Rad52, Rad54 and the breast cancer suppressor Brca2 (refs. 8,9).

Defective HDR in vertebrate cells provokes the instability of chromosome structure in dividing cells. Avian DT40 cells deficient in Rad51 perish rapidly as they divide, spontaneously accumulating broken and malformed chromosomes[10]. A similar phenotype occurs in DT40 or rodent cells lacking the Rad51 paralogs[11,12] and in murine cells deficient in Brca2 (ref. 13). This chromosomal instability is thought to stem from a failure to resolve DNA structures that arise during DNA replication[14]. For instance, HDR-deficient cells are highly sensitive to the clastogenic effects of replication-blocking drugs such as mitomycin C (MMC)[15,16], and there is evidence that they are unable to correctly process stalled DNA replication forks[17,18], consistent with observations made in bacteria and yeast[19–21]. Whether a similar function in the recovery of stalled forks is performed by HDR during unchallenged DNA replication is unclear, although the spontaneity of the chromosomal breakage that occurs in cells lacking Rad51, Brca2 or the Rad51 paralogs suggests that this is true[10,12,13,22]. Collectively, these observations indicate that DNA replication and recombination may be closely coordinated to maintain the fidelity of cell division.

However, the interplay between these DNA transactions during the vertebrate cell cycle is poorly understood. A major challenge to approaching this problem is the lack of methods available to rapidly ablate and complement proteins during cell-cycle progression. For instance, Rad51 depletion from DT40 cells using a tetracycline (tet)-regulable promoter occurs gradually over ~12–18 h[10], precluding the precise resolution of DNA replication from HDR. More than 20 years ago, Varshavsky's discovery of the N-end rule engendered a general method for rapid, temperature-sensitive, conditional protein degradation within 30–90 min[23,24]. An N-end rule protein degron has since been successfully applied to study replication in yeast[25] but has not previously been reported to work in vertebrate cells.

Here, we have created an N-end rule protein degron in the *Gallus gallus* cell line DT40, taking advantage of its capacity to grow at ambient temperatures ranging from 33–42 °C[26]. With this method, we have created a temperature-sensitive degron-RAD51 and used it to dissect the temporal progression of DNA replication and HDR during a single vertebrate cell cycle. We report that Rad51-dependent recombination is dispensable for replicative DNA synthesis but is instead

The Medical Research Council Cancer Cell Unit, Hutchison/MRC Research Centre, Hills Road, Cambridge CB2 0XZ, UK. Correspondence should be addressed to A.R.V. (arv22@cam.ac.uk).

Received 25 February; accepted 12 August; published online 14 September 2008; doi:10.1038/nsmb.1490

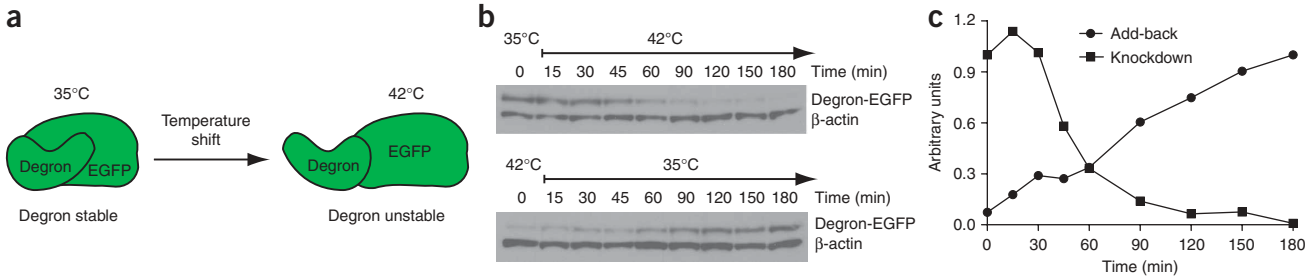

Figure 1 A thermosensitive conditional N-end rule degron in DT40 cells. (**a**) Schematic diagram of degron-EGFP. The protein is stable at 35 °C but undergoes N-terminal destabilization and degradation at the nonpermissive temperature, 42 °C. (**b**) Immunoblots showing the change in expression over time of degron-EGFP in whole-cell extracts from transfected cells. β-actin is used as a loading control. Above, degron-EGFP is depleted after shifting from 35 °C to 42 °C. Below, degron-EGFP is 'added back' when shifting from 42 °C back to 35 °C. (**c**) Quantification of degron-EGFP expression by densitometry. Protein levels are plotted in arbitrary units on the vertical axis, against time. For depletion, protein levels were normalized to expression at 0 min (at the permissive temperature) whereas for add-back, levels were normalized to the protein level at 180 min (also at the permissive temperature).

required in the G2 gap phase for entry into mitosis. The separation we observe between replicative DNA synthesis and Rad51-dependent HDR suggests a model in which the G2 phase of the vertebrate cell cycle is used to resolve DNA structures created in the wake of DNA replication that would otherwise impede mitosis.

RESULTS

Application of an N-end degron to vertebrate cells

An N-end rule degron form of the enhanced green fluorescent protein (EGFP) gene was created by fusing to its 5′ end the murine dihydrofolate reductase (DHFR) gene harboring a proline to leucine change at position 66, a mutation previously reported to cause the temperature-sensitive unfolding and degradation of the DHFR protein[23] via Varshavsky's N-end rule (**Fig. 1a**). Transfer of degron-EGFP expressing DT40 cells to the nonpermissive temperature of 42 °C rapidly depletes the protein to ~10% of the initial levels within 90 min and within 120 min leads to the absence of detectable protein (**Fig. 1b,c**). Conversely, shifting degron-EGFP–depleted cells back to the permissive temperature of 35 °C allows efficient recovery to the predepletion level within 150 min. Collectively, these data provide a general method to use an N-end rule protein degron in the DT40 cell line.

Degron-RAD51 supports cell growth

A degron-RAD51 fusion protein was introduced into a DT40 cell line[10] harboring a biallelic disruption of the *Gallus gallus RAD51* locus, in which nullizygosity for avian Rad51 has been functionally complemented by a tet-regulable operon (tetRAD51) expressing wild-type human RAD51 protein ($Rad51^{-/-(tetRAD51)}$), to create a cell line with the genotype $Rad51^{-/-(tetRAD51)(degRAD51)}$. Both tetRAD51 and degron-RAD51 are conditionally expressed; hereafter, '+' or '–' symbols are used against the genotype to indicate their presence or absence.

Rad51 nullizygosity triggers growth arrest and cell death[10], and thus treatment of $Rad51^{-/-(tetRAD51)}$ cells with doxycyline to turn off the tet-regulable *RAD51* prevents proliferation in culture (**Fig. 2a**, compare

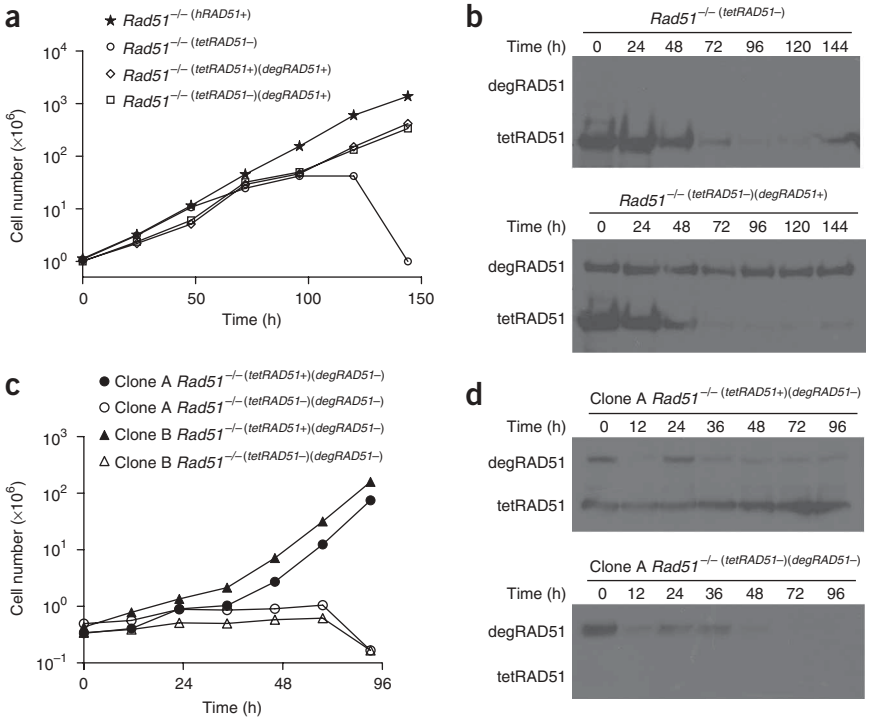

Figure 2 Degron-RAD51 supports cell viability. (**a**) Cell-proliferation curves show that expression of degron-RAD51 alone can prevent inviability and growth arrest in $Rad51^{-/-(tetRAD51-)(degRAD51+)}$ cells lacking other forms of RAD51. In contrast, RAD51-deficient $Rad51^{-/-(tetRAD51-)}$ are unable to proliferate. Controls show that expression of tetRAD51 alone, or coexpression tetRAD51 with degron-RAD51 (degRAD51), also supports cell growth. The number of viable cells is plotted on the vertical axis, against time. (**b**) Immunoblots showing changes in tetRAD51 and degron-RAD51 expression over time in whole-cell lysates from $Rad51^{-/-(tetRAD51-)}$ or $Rad51^{-/-(tetRAD51-)(degRAD51+)}$ cells treated as described in **a**. (**c**) Inactivation of degron-RAD51 by temperature shift to 42 °C in two independent clones (A and B) of cells expressing no other form of RAD51 results in growth arrest. (**d**) Immunoblots showing changes in tetRAD51 or degron-RAD51 expression over time in whole-cell lysates from $Rad51^{-/-(tetRAD51+)(degRAD51-)}$ or $Rad51^{-/-(tetRAD51-)(degRAD51-)}$ cells treated as described in **c**.

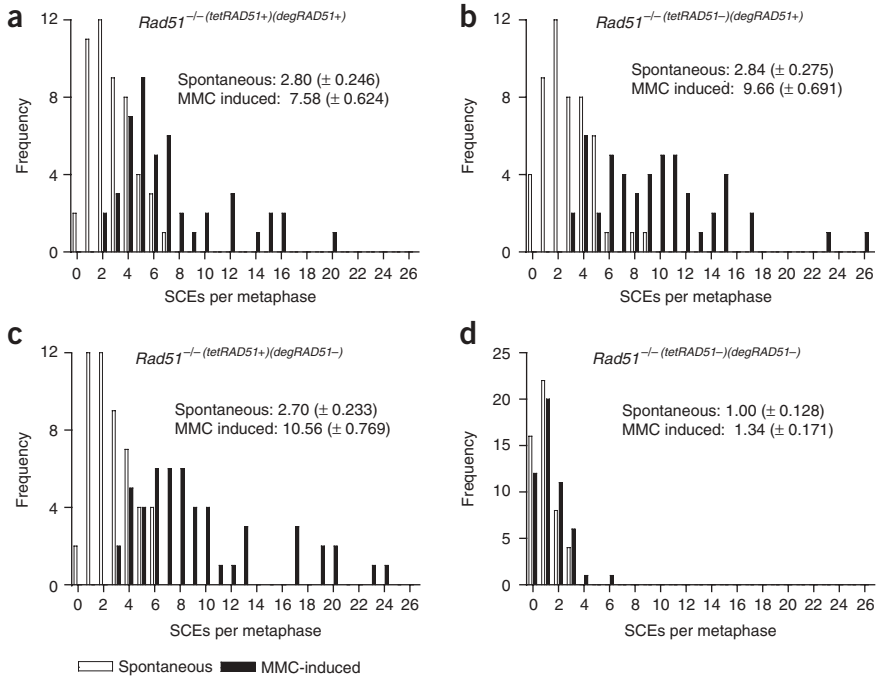

Figure 3 Degron-RAD51 supports sister-chromatid exchange (SCE). Histograms showing the frequency distribution of spontaneous (open bars) and MMC-induced (black bars) sister chromatid exchange (SCE) in control cells (**a**–**c**) expressing tetRAD51 and/or degron-RAD51, compared with RAD51-deficient $Rad51^{-/-(tetRAD51–)(degRAD51–)}$ cells (**d**). The mean number of SCEs per metaphase (± s.e.m.) for each histogram is indicated. At least 50 metaphases were examined per sample, and results are typical of two independent repeats.

$Rad51^{-/-(tetRad51+)}$ with $Rad51^{-/-(tetRAD51–)}$). At 35 °C, expression of degron-RAD51 (**Fig. 2b**) did not affect the ability of the cells to proliferate in the presence of tetRAD51 but did rescue cell growth in the absence of tetRAD51 (compare $Rad51^{-/-(tetRAD51+)(degRAD51+)}$ with $Rad51^{-/-(tetRAD51–)(degRAD51+)}$). Furthermore, two independently derived clones of $Rad51^{-/-(tetRAD51–)(degRAD51–)}$ cells failed to survive when shifted to the nonpermissive temperature of 42 °C (**Fig. 2c**), depleting degron-RAD51 (**Fig. 2d**). Thus, degron-RAD51 can functionally complement the essential requirement for Rad51 in maintaining the growth and viability of DT40 cells.

Degron-RAD51 supports sister-chromatid exchange

To ensure that degron-RAD51 is functional in HDR, we measured spontaneous sister chromatid exchange (SCE) and its induction by treatment with MMC in four cell lines: $Rad51^{-/-(tetRAD51+)(degRAD51+)}$; $Rad51^{-/-(tetRAD51–)(degRAD51+)}$; $Rad51^{-/-(tetRAD51+)(degRAD51–)}$; and $Rad51^{-/-(tetRAD51–)(degRAD51–)}$ (**Fig. 3a–d**). SCE is the cytogenetic consequence of an HDR event[27], and hence its baseline level and enhancement by MMC directly reflect the integrity of this process[12]. In $Rad51^{-/-(tetRAD51+)(degRAD51+)}$, $Rad51^{-/-(tetRAD51–)(degRAD51+)}$ or $Rad51^{-/-(tetRAD51+)(degRAD51–)}$ cells, a similar baseline level of ~2.8 spontaneous SCEs per cell was significantly increased by 3-4 fold after MMC exposure ($P < 0.0001$ by unpaired two-tailed *t*-test analysis ($n = 50$ for each cell line)). Comparisons of SCEs between the four cell lines, with and without MMC treatment, revealed no significant difference between $Rad51^{-/-(tetRAD51–)(degRAD51+)}$ and $Rad51^{-/-(tetRAD51+)(degRAD51–)}$ cells in the formation of either spontaneous or MMC-induced SCEs ($P > 0.05$ by two-way ANOVA plus Bonferroni post-test). These findings show that the expression of degron-RAD51 alone suffices for levels of SCE formation indistinguishable from the wild type.

In contrast, $Rad51^{-/-(tetRAD51–)(degRAD51–)}$ cells showed a reduction in spontaneous SCE (mean ± s.e.m. = 1.00 ± 0.1278 per metaphase spread, $n = 50$) that was significantly different from the other cell lines ($P \leq 0.05$, paired, two-way ANOVA plus Bonferroni post-test), confirming that degron-RAD51 depletion impairs HDR (**Fig. 3d**). This was further substantiated by the failure to increase SCE formation when these cells were challenged with MMC.

Intact replicative DNA synthesis followed by G2 arrest

Whether DNA recombination is required for replication is unclear. Although tetRAD51 depletion from asynchronously dividing DT40 cells leads to accumulation with *4N* DNA content, tetRAD51 levels decline gradually, with evidence of DNA damage–induced checkpoint activation[10,28]. We therefore used the $Rad51^{-/-(tetRAD51)(degRAD51)}$ cell line to ask whether Rad51-dependent HDR was required for the replicative phase of a single vertebrate cell cycle (**Fig. 4**).

Cells synchronized with mimosine at the G1-S boundary were shifted to the nonpermissive temperature of 42 °C to deplete degron-RAD51, before release into the S phase with or without doxycycline treatment. In control $Rad51^{-/-(tetRAD51+)(degRAD51+)}$, $Rad51^{-/-(tetRAD51–)(degRAD51+)}$ or $Rad51^{-/-(tetRAD51+)(degRAD51–)}$ cells expressing tetRAD51 and/or degron-RAD51 (**Fig. 4a** and **Supplementary Fig. 1** online), completion of the S phase and entry into *4N* DNA content occurred between 6–8 h after release, with progression into the next cell cycle evident by 10–12 h.

Completion of the S phase was not impaired by the absence of RAD51 (**Fig. 4a**) in doxycycline-treated cells expressing neither tetRAD51 nor degron-RAD51 (that is, $Rad51^{-/-(tetRAD51–)(degRAD51–)}$ cells; **Fig. 4b**). However, these cells failed to enter a second cell cycle and, instead, remained arrested with *4N* DNA content even at 10 h after release. To confirm that this arrest occurs after the completion of detectable replicative DNA synthesis, we used a ^{3}H-^{14}C double-labeling procedure (**Fig. 4c**). In cells lacking RAD51, there was no detectable ^{3}H incorporation into genomic DNA by 6 h after release, confirming that bulk DNA synthesis was indeed complete at this time, consistent with *4N* DNA content (**Fig. 4a**). In addition, the distribution of ^{3}H incorporation over time showed that RAD51-depleted cells reach mid–S phase 2.66 ± 0.11 h (mean ± s.e.m.) after release, compared to 2.77 ± 0.35 h (mean ± s.e.m.) in the presence of RAD51 (data not shown), suggesting that neither the extent nor the kinetics of replicative DNA synthesis were grossly altered by the absence of RAD51-dependent HDR. Taken together, our results demonstrate that replicative DNA synthesis can be completed in a single vertebrate cell cycle, despite the lack of RAD51.

Our findings also confirm that a functional recombination machinery is required for timely transit from the G2 phase into

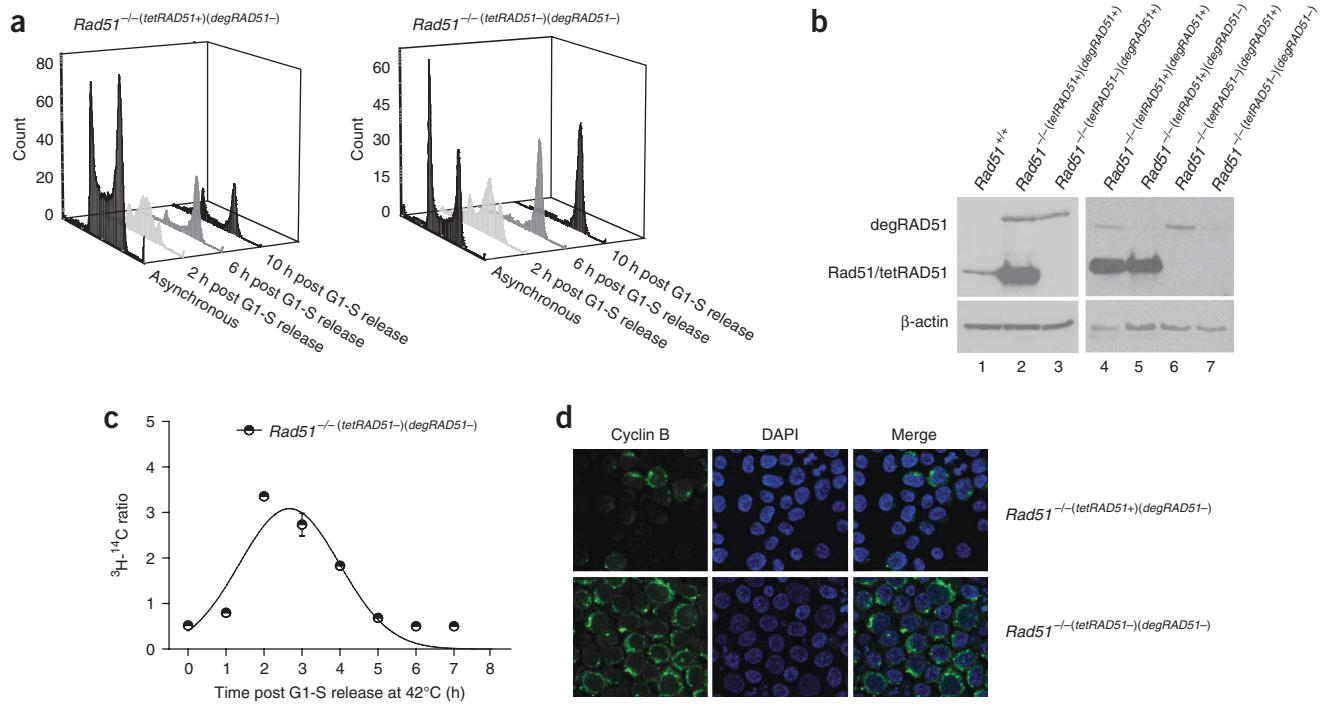

Figure 4 RAD51 is dispensable for replicative DNA synthesis but becomes essential after replication for mitotic entry. (**a**) Cell-cycle profiles of *Rad51*$^{-/-(tetRAD51+)(degRAD51-)}$ and *Rad51*$^{-/-(tetRAD51-)(degRAD51-)}$ cells at the nonpermissive temperature are shown. DNA content measured by propidium iodide staining and flow cytometry is plotted on the horizontal axis, against relative cell number. Cells were synchronized at the G1-S boundary using mimosine before release into the S phase[56]. Cells lacking degron-RAD51 (degRAD51) transit the S phase with similar kinetics to cells expressing tetRAD51, only to arrest with *4N* DNA content. (**b**) Immunoblots for the expression of RAD51 and β-actin in whole-cell lysates from wild-type cells (lane 1), *Rad51*$^{-/-(tetRAD51+)(degRAD51+)}$ cells (lane 2) and *Rad51*$^{-/-(tetRAD51-)(degRAD51+)}$ cells (lane 3) show that the level of degron-RAD51 expression is comparable with endogenous Rad51. Lanes 4 to 7 compare expression in asynchronous cultures of *Rad51*$^{-/-(tetRAD51+)(degRAD51+)}$ cells (lane 4) or *Rad51*$^{-/-(tetRAD51-)(degRAD51+)}$ cells (lane 6) with expression in cells synchronized with mimosine at 42 °C (lanes 5, 7), the nonpermissive temperature at which degron-RAD51 is depleted. (**c**) Ratio of ^{3}H-^{14}C incorporation in *Rad51*$^{-/-(tetRAD51-)(degRAD51-)}$ cells after synchronization and release into the S phase at 42 °C. Cells lacking RAD51 complete replication in <6 h, as do wild-type cells. ^{3}H-^{14}C ratio values were fitted to a Gaussian distribution curve. Cells reach midreplication with similar kinetics in the absence or presence of RAD51 (data not shown) at 2.66 ± 0.11 h, $n = 2$ or 2.77 ± 0.35 h, $n = 2$ (mean ± s.e.m.), respectively. Mean values were compared by a two-tailed unpaired *t*-test confirming there was no significant difference ($P = 0.51$) in replication progression. (**d**) Immunofluorescence staining of *Rad51*$^{-/-(tetRAD51+)(degRAD51-)}$ or *Rad51*$^{-/-(tetRAD51-)(degRAD51-)}$ cells for cyclin B localization 8 h after release into the S phase. In cells lacking RAD51 (below), cyclin B stains in the cytosol but not in the nucleus, characteristic of cells in G2 phase (note also the increase in nuclear size shown by DAPI staining). In contrast, cells expressing tetRAD51 (above) show heterogeneous cyclin B staining typical of asynchronous cultures (see cell-cycle profiles in **Figure 4a**).

mitosis, owing to DNA damage–induced checkpoint activation[28]. *Rad51*$^{-/-(tetRAD51-)(degRAD51-)}$ cells at 8 h post-release, arrested with *4N* DNA content, showed a typical G2 distribution of cyclin B staining (**Fig. 4d**), maintained intact nuclear envelopes, lacked morphological signs of chromosome condensation and did not stain for the mitotic marker histone H3 phosphorylated on serine 10 (data not shown). Moreover, treatment with caffeine, an inhibitor of ATM, ATR and other kinases that mediate G2-checkpoint enforcement, allows progression into mitosis[28] (**Supplementary Fig. 2** online). Notably, caffeine-treated RAD51-deficient cells entered a second round of DNA replication, before arresting once again with *4N* DNA content. Hence, RAD51 depletion during the S phase blocks mitotic entry through activation of the G2 checkpoint, which monitors replicated DNA for the presence of DNA structures that might impair chromosome segregation within a single cell cycle, consistent with previous results[10,28].

RAD51 add-back after DNA replication overcomes G2 arrest

Next, we took advantage of the thermosensitive degron system to 'add-back' degron-RAD51 to RAD51-deficient *Rad51*$^{-/-(tetRAD51-)(degRAD51-)}$ cells at different times during a single cell cycle by shifting cells to the permissive temperature of 35 °C (**Fig. 5a**). Degron-RAD51 expression is quickly restored to predepletion levels ~40 min after the shift (**Fig. 5b**). Add-back at 4 h, 6 h or 8 h after release into the S phase, corresponding to the S, late S or G2 phases, was sufficient to overcome the block to mitotic entry provoked by RAD51 depletion. However, add-back of RAD51 10 h after release into the S phase failed to promote mitosis. These findings indicate that Rad51-dependent HDR becomes essential in a discrete window of time during the cell cycle, between 8 h and 10 h after release into the S phase, corresponding to a period when cells have already entered the G2 phase but before prolonged G2 arrest. Consistent with the notion that RAD51 is required in G2 only after the completion of replication, degron-RAD51 add-back at 8 h after release was not accompanied by detectable DNA synthesis, as measured by the ratio of ^{3}H-^{14}C incorporation (**Fig. 5c**). Thus, taken together, our observations suggest that the recombination machinery becomes essential in G2 to resolve DNA structures that would otherwise impede mitosis.

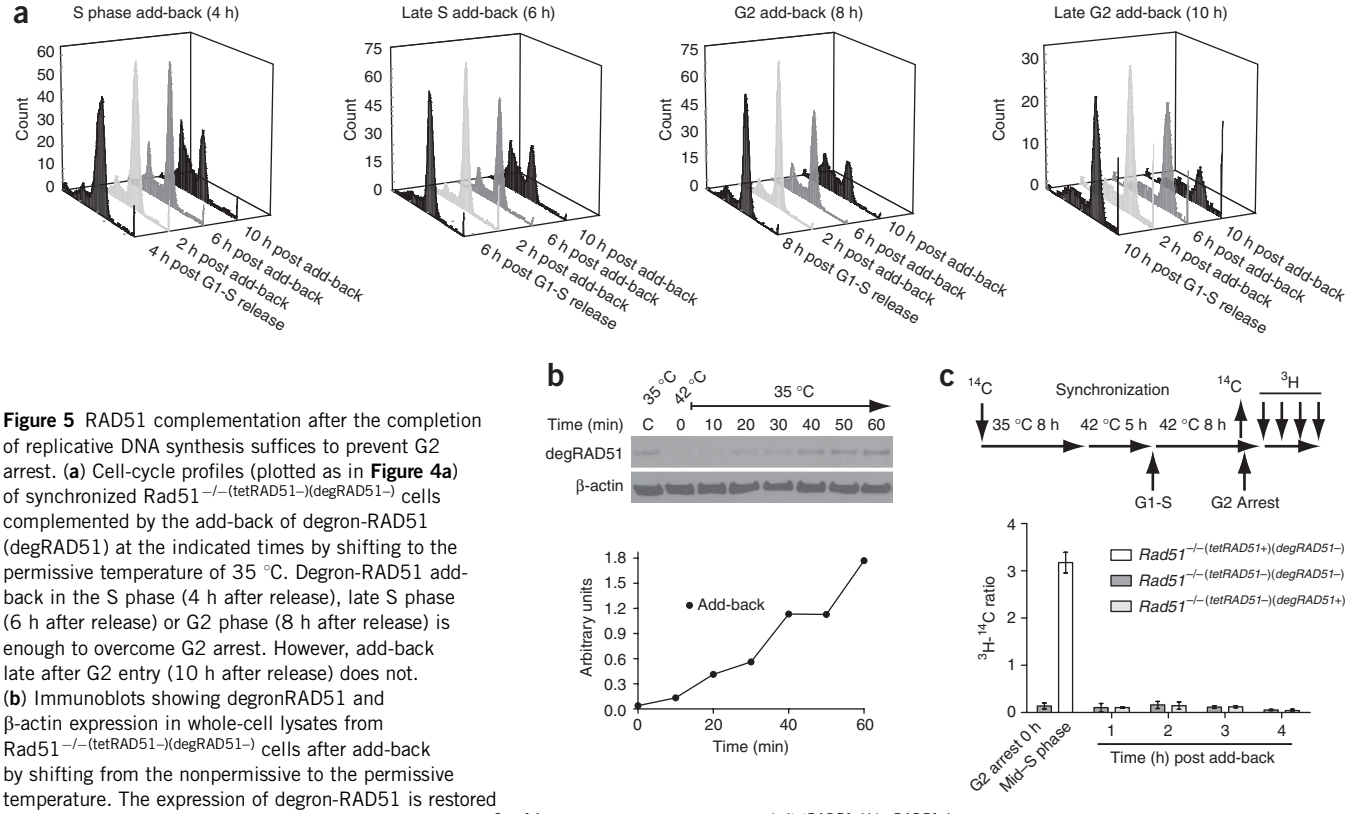

Figure 5 RAD51 complementation after the completion of replicative DNA synthesis suffices to prevent G2 arrest. (**a**) Cell-cycle profiles (plotted as in **Figure 4a**) of synchronized Rad51$^{-/-(tetRAD51-)(degRAD51-)}$ cells complemented by the add-back of degron-RAD51 (degRAD51) at the indicated times by shifting to the permissive temperature of 35 °C. Degron-RAD51 add-back in the S phase (4 h after release), late S phase (6 h after release) or G2 phase (8 h after release) is enough to overcome G2 arrest. However, add-back late after G2 entry (10 h after release) does not. (**b**) Immunoblots showing degronRAD51 and β-actin expression in whole-cell lysates from Rad51$^{-/-(tetRAD51-)(degRAD51-)}$ cells after add-back by shifting from the nonpermissive to the permissive temperature. The expression of degron-RAD51 is restored within ~40 min after the temperature shift. (**c**) Ratio of ^{3}H-^{14}C incorporation in Rad51$^{-/-(tetRAD51-)(degRAD51-)}$ cells after degron-RAD51 add-back by shifting to the permissive temperature at 8 h after release into the S phase. Incorporation was determined every hour over the course of 4 h. Although degron-RAD51 add-back at 8 h after release is enough to prevent G2 arrest, it is not accompanied by any detectable DNA synthesis.

ssDNA structures accumulate after RAD51 depletion

Several lines of evidence indicate that G2-checkpoint activation after DNA replication in the absence of RAD51 is triggered by the accumulation of DNA structures marked by ssDNA and the activation of the ssDNA binding protein, RPA32. In synchronized RAD51-deficient *Rad51*$^{-/-(tetRAD51-)(degRAD51-)}$ cells (but not in three control cell lines expressing tetRAD51 and/or degron-RAD51), using a nondenaturing immunofluorecence procedure, we detected focal staining of ssDNA labeled with bromodeoxyuridine (BrdU) in the G2 phase, QJ; 8 h after release from mimosine arrest (**Fig. 6a**, second column). RPA32 is reported to accumulate at ssDNA tracts and to undergo phosphorylation signifying activation of downstream responses such as the G2 checkpoint[29–31]. Indeed, nuclear foci containing the Thr21-phosphorylated form of RPA32 (p-RPA) costained with the anti-BrdU–stained ssDNA tracts (**Fig. 6a**, third column), indicating that these regions of ssDNA marked by BrdU foci are indeed recognized by the G2-checkpoint machinery. The structures marked by anti-BrdU and anti–p-RPA staining are unlikely to represent double-stranded DNA breaks (DSBs). Using a nondenaturing Comet assay performed on RAD51-deficient *Rad51*$^{-/-(tetRAD51-)(degRAD51-)}$ cells 8 h after release into the S phase, corresponding to the peak of anti-BrdU staining, we failed to detect the 'tails' typical of DSBs (**Supplementary Fig. 3** online). Finally, focal anti-BrdU ssDNA staining gradually accumulated (**Fig. 6b**) in synchronized RAD51-deficient *Rad51*$^{-/-(tetRAD51-)(degRAD51-)}$ cells during DNA replication to reach a peak 8 h after release, corresponding, as previously noted (**Fig. 4a**,**d**), to the G2 phase. This pattern of accumulation is suggestive of DNA structures engendered during replicative DNA synthesis whose resolution requires an intact recombination machinery.

RAD51 resolves ssDNA structures during G2

The add-back of degron-RAD51 in a discrete time window after replicative DNA synthesis is enough to prevent G2 arrest (**Fig. 5a**). We therefore asked whether add-back could also resolve any accumulated ssDNA structures marked by anti-BrdU foci. This was indeed the case (**Fig. 7a**), linking the resolution of these structures by a RAD51-dependent mechanism with competence to enter mitosis. This conclusion is supported by the colocalization of degron-RAD51 after add-back with anti-BrdU–stained ssDNA foci (**Fig. 7b**).

During which cell-cycle phase(s) does Rad51-dependent HDR become necessary to resolve ssDNA structures generated during replication? Over the course of a single cell cycle, we monitored the formation of foci containing anti-BrdU–stained ssDNA, p-RPA or degron-RAD51 in *Rad51*$^{-/-(tetRAD51-)(degRAD51-)}$ cells either devoid of RAD51 (**Fig. 7c**) or after degron-RAD51 add-back during G2 (**Fig. 7d**) or in the S phase (**Fig. 7e**). In the absence of RAD51, we observed accumulation of foci beginning from late S phase until the end of replication in G2 (**Fig. 7c**). Degron-RAD51 add-back in G2 leads to the accumulation of degron-RAD51 foci, which correlated with a gradual decline in the number of foci stained with anti-BrdU or anti–p-RPA (**Fig. 7d**). Notably, even when degron-RAD51 is added back during the S phase, the number of p-RPA foci continued to increase until the end of replicative synthesis in G2, and only then declined (**Fig. 7e**). Moreover, the number of degron-RAD51 foci still

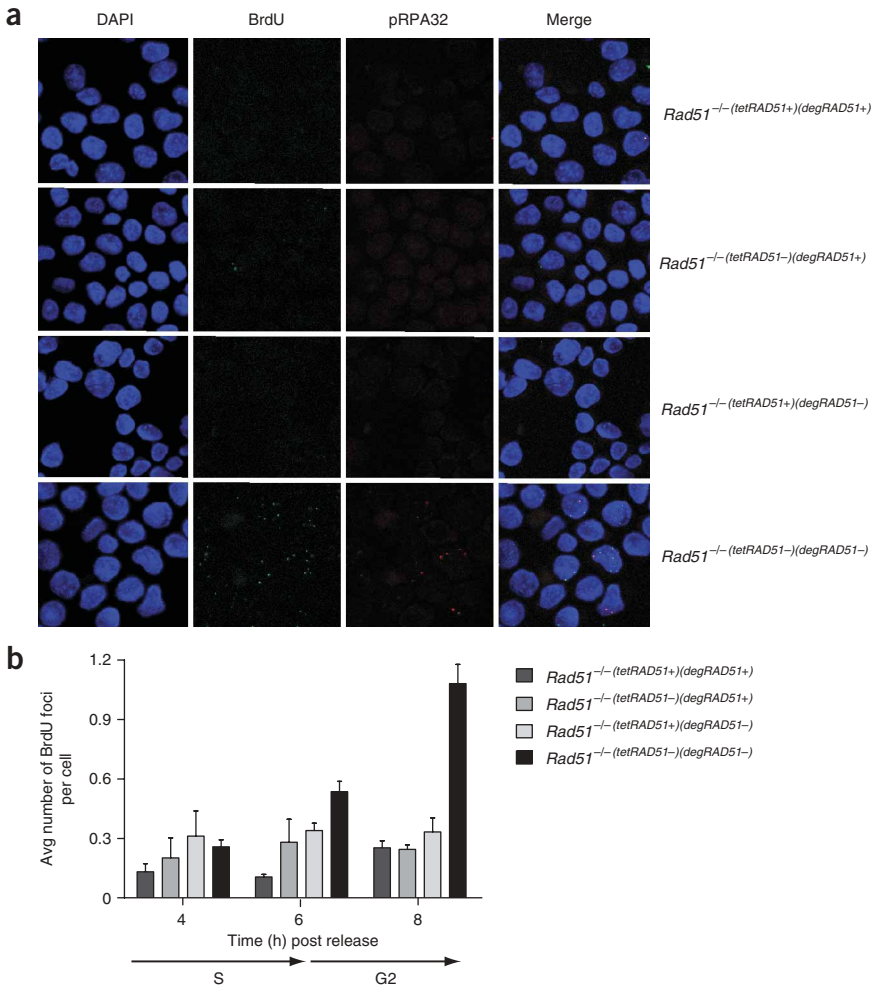

Figure 6 ssDNA structures marked by anti–p-RPA staining accumulate in the first cell cycle without RAD51. (**a**) Immunofluorescence analysis under nondenaturing conditions of synchronized cells 8 h after release into the S phase. DAPI marks cell nuclei (first column), anti-BrdU detects ssDNA tracts (second column) and the third column shows anti–phospho (p)-RPA32 staining. Representative images are shown. At this time point, foci of anti-BrdU and anti–p-RPA staining indicative of ssDNA tracts are abundant only in the RAD51-deficient *Rad51*$^{-/-(tetRAD51-)(degRAD51-)}$ cells (lowermost) but not in controls expressing tetRAD51 and/or degron-RAD51. Note the coincidence in the merged image (final column) of anti-BrdU and anti–p-RPA staining in foci. (**b**) Enumeration of anti-BrdU ssDNA foci in synchronized control cells expressing tetRAD51 and/or degron-RAD51, compared with *Rad51*$^{-/-(tetRAD51-)(degRAD51-)}$ cells lacking RAD51, at different times after release from mimosine arrest during a single cell cycle. At least 500 cells were analyzed for each time point by automated microscopy. The average number of foci per cell (± s.e.m.) is plotted against time after release into the S phase.

peaked in G2 even after add-back in the S-phase, despite the expected restoration of predepletion levels of degron-RAD51 within ~40 min of add-back (**Fig. 5b**). We interpret these patterns to suggest that ssDNA structures associated with replication are preferentially resolved during the G2 phase after the completion of replicative synthesis, consistent with a temporal separation between DNA replication and the culmination of homologous recombination.

Rad51 and p-RPA colocalize during G2 in wild-type cells

Our findings thus far demonstrate that depletion of degron-RAD51 leads to the appearance of ssDNA structures during replication that can be preferentially resolved during G2 to allow entry into mitosis. Do similar structures appear during replication in wild-type, Rad51-proficient cells? If so, does their resolution also occur predominantly in the G2 phase? To address these questions, we monitored the appearance and colocalization of foci containing p-RPA or Rad51 in wild-type DT40 cells synchronized in the mitotic metaphase by nocodazole treatment, before release into the cell cycle (**Fig. 8a**). Synchronized cells transited the S phase 2–6 h after release from mitotic synchronization ('M release') and entered a second cell cycle 10 h after release. The number of foci containing p-RPA or RAD51 increased throughout the S phase, peaked during G2 transit and declined during entry into the next cell cycle (**Fig. 8b**). Notably, the colocalization of Rad51 staining with p-RPA foci increased markedly from 13.1 ± 4.6% (mean ± s.e.m., $n = 6$) during late S phase (6 h after release) to 60.1 ± 7.7% (mean ± s.e.m., $n = 7$) at G2 (8 h after release) (**Fig. 8c**). These differences are statistically significant ($P < 0.0001$, one-way ANOVA followed by Dunn's comparison post-test). Thus, our results suggest that ssDNA structures marked by p-RPA accumulate during unchallenged DNA replication in wild-type cells, to be preferentially resolved during the G2 phase when there is maximal colocalization of p-RPA with Rad51. These findings, consistent with our observations in RAD51-deficient *Rad51*$^{-/-(tetRAD51-)(degRAD51-)}$ cells, suggest that DNA replication and HDR are temporally separated during the vertebrate cell cycle.

Evolution of chromosomal lesions

HDR deficiency provokes chromosomal aberrations, but how they evolve is uncertain. For instance, the gradual depletion of tetRAD51 from DT40 cells over several asynchronous cell cycles predominantly causes isochromatid breaks, spanning both sister chromatids, rather than chromatid-type lesions affecting just one of them[10]. We have exploited the degron-RAD51 system to track the evolution of broken chromosomes during successive cell cycles in the absence of a functional HDR machinery. Mimosine-arrested cells synchronously released into the S phase were driven into mitosis using colcemid, and then the number and types of lesions in condensed chromosomes was quantified and assessed in metaphase spreads. **Table 1** compares the number of chromatid versus isochromatid breaks in three control cell lines expressing tetRAD51 and/or degron-RAD51 with those in *Rad51*$^{-/-(tetRAD51-)(degRAD51-)}$ cells, during the first or second cell cycles. In RAD51-deficient cells, entry into a second cell cycle without RAD51 was stimulated by caffeine-induced suppression of the G2 checkpoint.

RAD51-deficient *Rad51*$^{-/-(tetRAD51-)(degRAD51-)}$ cells showed an overall increase in the number of chromosomal lesions compared to controls in the first cell cycle. Unexpectedly, there was a three-fold preponderance of chromatid over isochromatid breakage. Breaks

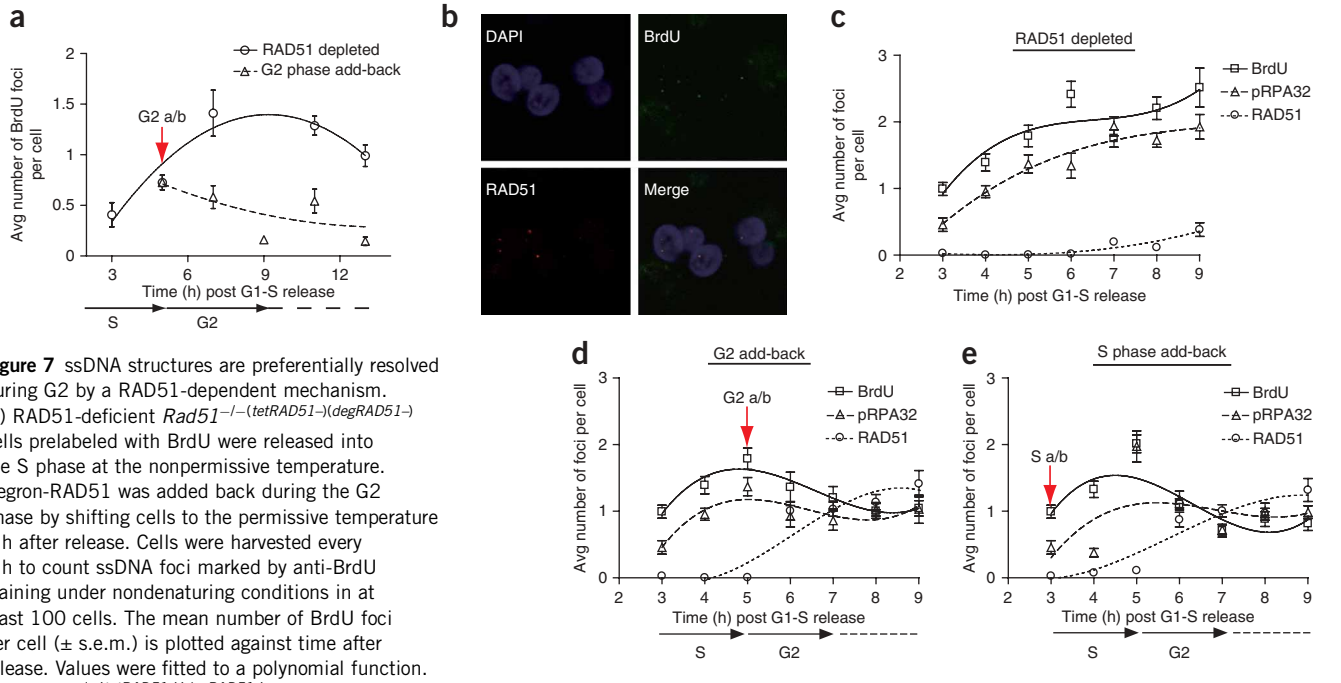

Figure 7 ssDNA structures are preferentially resolved during G2 by a RAD51-dependent mechanism. (**a**) RAD51-deficient *Rad51*$^{-/-(tetRAD51-)(degRAD51-)}$ cells prelabeled with BrdU were released into the S phase at the nonpermissive temperature. Degron-RAD51 was added back during the G2 phase by shifting cells to the permissive temperature 5 h after release. Cells were harvested every 2 h to count ssDNA foci marked by anti-BrdU staining under nondenaturing conditions in at least 100 cells. The mean number of BrdU foci per cell (± s.e.m.) is plotted against time after release. Values were fitted to a polynomial function. (**b**) *Rad51*$^{-/-(tetRAD51-)(degRAD51-)}$ cells treated as in **a** above to add back degron-RAD51 during the G2 phase were immunostained with anti-RAD51 (red) and anti-BrdU (green) antibodies 2 h after degron-RAD51 add back. Degron-RAD51 staining colocalizes with anti-BrdU–stained ssDNA foci. (**c**) RAD51-deficient *Rad51*$^{-/-(tetRAD51-)(degRAD51-)}$ cells kept at the nonpermissive temperature were harvested hourly and stained under nondenaturing conditions with anti-BrdU, anti–p-RPA32 or anti-RAD51. Foci were enumerated in a minimum of 100 cells at each time point. The average number of foci per cell (± s.e.m.) is plotted against time after release. Values were fitted to a polynomial function. (**d**,**e**) The effects on foci formation of degron-RAD51 add-back at 3 h or 5 h after release from mimosine arrest, corresponding to mid–S phase (**e**) or G2 (**d**). Foci were enumerated, and the results are presented as in **c**.

affecting a single chromatid typically arise from the failure of post-replication repair[32], further supporting our proposal that HDR works after replication during G2 to repair lesions that would otherwise impede mitosis. Notably, and in contrast to the first cell cycle without RAD51, there is an approximately 1.6-fold excess of isochromatid breakage by the end of the second cell cycle. Thus, our findings suggest that chromosomal lesions in vertebrate cells devoid of a functional HDR machinery evolve in two steps. Chromatid lesions engendered by the failure of post-replication repair during the first cell cycle evolve into the isochromatid breaks previously reported in asynchronous RAD51-depleted cells[10] only during a second round of DNA replication[33].

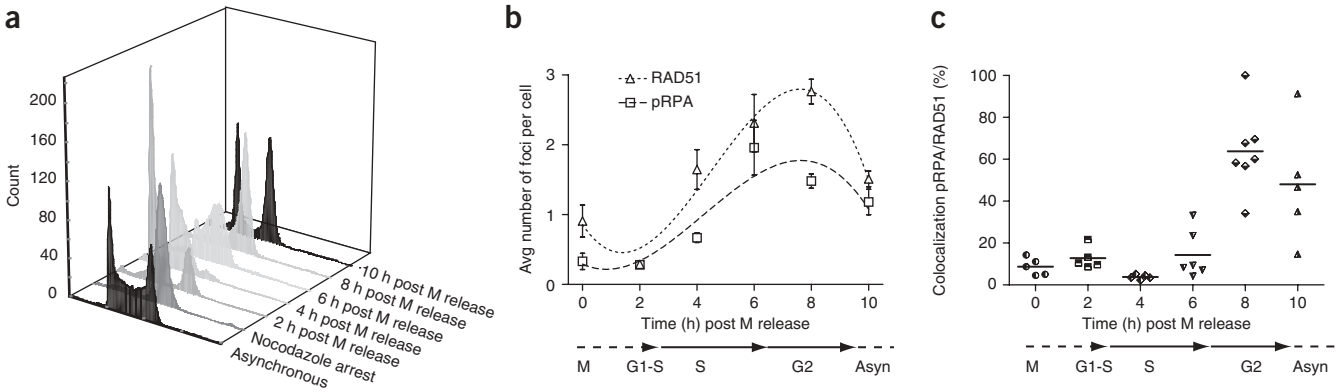

Figure 8 ssDNA foci accumulate during unchallenged replication in wild-type cells and colocalize with RAD51 foci preferentially during G2. (**a**) Cell-cycle profiles (plotted as in **Figure 4a**) of wild-type DT40 (clone 18) cells, synchronized in the mitotic metaphase with nocodazole, before release into the cell cycle. (**b**) Nocodazole-arrested cells released synchronously into cycle were harvested at different times after release and immunostained with anti-RAD51 and anti-p-RPA. Foci were enumerated in a minimum of 50 cells (within a minimum of five fields) at each time point. The average number of foci per cell (± s.e.m.) is plotted against time after release. Values were fitted to a polynomial function. (**c**) The percentage of p-RPA foci colocalizing with RAD51 at the indicated time points is plotted against time after release. There is a statistically significant difference between cells in G2 versus the S phase ($P < 0.0001$, one-way ANOVA followed by Dunn's multiple comparison post-test). Maximal colocalization occurs during G2 (60.1 ± 7.7%, mean ± s.e.m., $n = 5$) and is significantly higher than during the S phase at 2 h (13 ± 2.1%, mean ± s.e.m., $n = 5$), 4 h (3.2 ± 0.3%, mean ± s.e.m., $n = 5$) or 6 h (13.1 ± 4.5%, mean ± s.e.m., $n = 6$) after release.

Table 1 Evolution of chromosomal lesions during the first and second cell cycles without RAD51

	First cell cycle		Second cell cycle	
Genotype	Chromatid type	Isochromatid type	Chromatid type	Isochromatid type
tetRAD51+, degRAD51+	0.22 (± 0.046)	0.04 (± 0.020)	0.22 (± 0.059)	0.08 (± 0.048)
tetRAD51–, degRAD51+	0.22 (± 0.044)	0.04 (± 0.020)	0.24 (± 0.061)	0.08 (± 0.039)
tetRAD51+, degRAD51–	0.27 (± 0.053)	0.06 (± 0.024)	0.24 (± 0.073)	0.16 (± 0.052)
tetRAD51–, degRAD51–	0.48 (± 0.058)	0.14 (± 0.034)	0.72 (± 0.114)	1.12 (± 0.120)

The mean number of chromatid or isochromatid breaks per metaphase (± s.e.m.) is shown. At least 50 metaphases were enumerated per sample. Results are typical of at least two independent experiments. RAD51-deficient cells show a statistically significant increase in the overall number of chromosomal lesions in the first cell cycle compared to controls ($P \leq 0.05$, one-way ANOVA plus Dunn's multiple comparison post-test), with a 3.3-fold preponderance of chromatid breaks affecting a single sister chromatid. In the second cell cycle, RAD51-deficient cells show a 1.6-fold excess of isochromatid breaks, affecting both sister chromatid arms.

DISCUSSION

We describe here a method to exploit Varshavsky's N-end rule for conditional genetics in vertebrate cells and the use of this method to dissect the coordination of DNA replication and HDR in a single cell cycle. We provide several lines of evidence supporting a model for the vertebrate cell cycle in which HDR is temporally segregated during the G2 phase from replicative DNA synthesis in the S phase and chromosome segregation in the M phase. Our findings have several implications.

Our data provide direct evidence that HDR is dispensable for the completion of bulk DNA synthesis during the S phase (**Fig. 4**) of a single vertebrate cell cycle. It remains formally possible that Rad51-independent replication remains incomplete through specific genomic regions with specialized structures, such as replication-fragile loci[34]. This is beyond the sensitivity of our methods to detect, but the vast majority of the vertebrate genome can clearly be replicated without Rad51. This is contrary to the expectation from studies on prokaryotic cells, where HDR is essential for the reassembly of functional replisomes at stalled or collapsed forks[21,35–37]. Whether this is also true in simple eukaryotes like yeast is currently unclear. On the one hand, genetic studies reveal that the viability of many replication- or replication-checkpoint yeast mutants depends on HDR, indicating that recombination does help to resume stalled replication[38]. On the other hand, yeast Rad51 (unlike in vertebrates) is essential for neither cell proliferation nor maintenance of genome integrity during replication[10,39–41]. Thus, our findings highlight differences between when and how recombination may be used to deal with replication-associated DNA structures in prokaryotes, yeast and vertebrate cells.

Passage through a single, unchallenged round of DNA replication in the absence of Rad51 causes a checkpoint-mediated G2 arrest (**Fig. 4a**,**d**), accompanied by the accumulation of foci containing ssDNA tracts and the activated form of RPA (**Fig. 6**). This suggests that, in vertebrates, HDR is crucial to process at least one type of replication-associated DNA structure that cannot be resolved by alternative mechanisms, such as translesion synthesis[42], and whose persistence would otherwise impede progression through mitosis.

However, not all DNA lesions created during replication may benefit from processing via HDR. For example, cells deficient in the HDR mediator Xrcc2 arrest with *4N* DNA content in their first cell cycle after treatment with the alkylating agent *N*-methyl-*N*′-nitro-*N*-nitrosoguanidine (MNNG), accumulating ssDNA lesions generated via the mismatch repair pathway, whereas recombination-proficient control cells arrest in their second cell cycle but with the accumulation of DSBs. In this situation, HDR may convert mismatch-repair intermediates into a 'checkpoint-silent' form, bypassing G2-checkpoint activation in the first cell cycle, only for DNA breaks to form during the second[43,44].

The precise nature of the DNA structures that accumulate during replication without Rad51 is unclear. Work in yeast raises some possibilities. After replication stress induced by hydroxyurea, budding yeast strains deficient in the replication-checkpoint kinase Rad53 accumulate two classes of aberrant replication intermediates visualized by EM[45]. The majority (75%) comprise up to 800 nt of ssDNA on both the leading and lagging strands, corresponding to hemireplicated or gapped molecules. A second class, observed at ~10% of forks in checkpoint-defective cells, comprised X-shaped molecules with one free end corresponding to a regressed replication fork[46]. Similar experiments to visualize DNA replication intermediates in vertebrate cells are precluded by technical challenges. However, because no detectable DNA synthesis seems to be required to resolve the structures we detected (**Fig. 5c**), they are unlikely to correspond to hemireplicated or gapped molecules. Instead, their dependence on Rad51-dependent HDR for resolution (**Fig. 7d,e**) suggests that they may represent structures similar to regressed forks.

Notably, the absence of Rad51 in a single cell cycle causes a preponderance of chromatid breaks over isochromatid lesions (**Table 1**), in contrast to work in which Rad51 is gradually depleted[10]. Not only does this support our proposal that Rad51-mediated HDR resolves specific replication-associated structures after replicative synthesis[32], but it also exemplifies the ability of the degron system to temporally dissect cell-cycle events. We find that isochromatid lesions begin to accumulate only in the second cell cycle, so their genesis may require DNA replication.

Data from yeast suggest that unscheduled HDR during the S phase can lead to the generation of DNA lesions at stalled DNA replication forks[47–50] and that the Cds1-mediated checkpoint is essential to prevent this. Thus, Cds1-deficient fission yeast strains show the inappropriate colocalization of Rad22 foci with proliferating cell nuclear antigen (PCNA) in the S phase and the formation of Rhp51-dependent aberrant DNA structures, preventing the completion of bulk DNA synthesis[47]. It is plausible that there is a similar necessity in vertebrate cells to separate HDR from DNA replication.

Our work provides several lines of evidence that this is indeed the case. We not only show using degron-RAD51 that HDR becomes necessary only in G2 after the completion of DNA replication to allow mitotic entry (**Figs. 5** and **7**), but also that, in wild-type cells during unchallenged replication, p-RPA binding DNA structures that accumulate during the S phase are resolved preferentially during G2 (**Fig. 8b**). Moreover, in wild-type cells, Rad51 colocalizes with p-RPA primarily in G2 (**Fig. 8c**), further supporting the notion that Rad51-dependent HDR is invoked only after the completion of DNA

replication. Thus, our findings offer fresh insight into the coordination of DNA transactions during the vertebrate cell cycle and suggest that one biological purpose for the G2 gap phase is to separate homologous DNA recombination from DNA replication and chromosome segregation.

METHODS

Plasmid constructs. We created *pDegron-EGFP* by PCR amplifying the degron cassette from *pKL187* (ref. 51) using the primers *FOR*5′- GGCGCCGCTAG CATGCAGATTTTCGTCAAGACTTT-3′ and *REV*5′-GGCCGGTACCGAGTCT TTCTTCTCGTAGACTTCAAAC-3′, before digestion with NheI and KpnI and ligation into *pEGFP-N1* (Clontech). For PCR amplification of *pDegron-RAD51*, we used the primers *FOR*5′-GGCGGAGCGCTATGCAGATTTTCGTCAA GACTT-3′ and *REV*5′-GGCGTCGACTACCGAGTCTTTCTTCTCGTAGACTT-3′, digested the insert with AfeI and SalI, and ligated it into *GFP-RAD51* (ref. 52). All constructs were verified by nucleotide sequencing.

Cell culture and transfection. Transfection into wild-type Clone 18 DT40 cells was as previously described[10]. G418 geneticin sulfate (Gibco) was used for selection. *pDegron-RAD51*–transfected cells were selected at 35 °C. Degron depletion was carried out at 42 °C and complementation at 35 °C, and 10 ng ml^{-1} doxycycline hyclate (Sigma) was used to regulate tetRAD51 expression. Cells were synchronized at the G1-S boundary by treatment with 400 μm mimosine (Sigma) for 5 h. Mitotic synchronization was brought about with 500 ng ml^{-1} Nocodazole (Sigma) for 5 h. Caffeine (Sigma) was used at 2 mM for 2 h to suppress the G2 checkpoint.

Western blotting. Whole-cell extracts (WCEs) were prepared in ice-cold RIPA buffer (50 mM Tris-HCl, pH 7.4, 150 mM NaCl, 0.5% (v/v) deoxycholate, 0.1% (v/v) SDS and 1% (v/v) Nonidet P-40) supplemented with 1 mM DTT, 1 mM PMSF and protease inhibitors (Amersham). Protein concentration was quantified using the Biocinchonic Assay (Sigma). WCEs were resolved by 4–12% SDS-PAGE (Invitrogen) and transferred to nylon membranes (Millipore) before blotting with the appropriate antibodies: mouse monoclonal anti-EGFP JL-18 (BD Biosciences), rabbit polyclonal anti-RAD51 (Calbiochem), mouse monoclonal anti–β–actin (Sigma) and horsradish peroxidase (HRP)-conjugated secondary antibodies against rabbit and mouse used at a 1:20000 and 1:40000 dilution, respectively. Signal intensities were quantified by integrated density measurements on ImageJ (http://rsbweb.nih.gov/ij/).

Cell viability. DT40 cells were grown and maintained in log phase. Viable cells were enumerated after trypan blue staining using a Beckman Coulter Vicell XR Cell Viability analyzer.

Metaphase spreads and SCE analysis. We carried out SCE analysis as previously described[53]. Metaphase spreads were prepared by pulsing cells with 100 ng ml^{-1} colcemid for 3 h before preparation as for SCE, except that staining was for 1–2 min at room temperature (20–24 °C) with 3% (v/v) Giemsa (Invitrogen) diluted in 0.05 M sodium phosphate buffer, pH 6.8.

Cell-cycle analysis. DT40 cells (2×10^6) were resuspended in 0.5 ml of PBS before addition of 4.5 ml ice-cold 70% (v/v) ethanol and incubation for at least 2 h. Before analysis, cells were washed once with PBS, incubated in 1 ml of 20 μg ml^{-1} propidium iodide (Sigma), 50 μl ml^{-1}) RNase A and 0.1% (v/v) Triton X-100 in PBS for 15 min at 37 °C. Cell-cycle profiles were acquired on a FACSCalibur instrument (Becton Dickinson) using FACSDiva Software 6.0 (BD Biosciences).

Immunofluorescence microscopy. To detect ssDNA foci, cells were labeled with 10 μm BrdU (Sigma) during synchronization and release into the S phase, harvested at the indicated time points, spun onto poly-L-lysine slides by Cytospin centrifugation and air-dried at 37 °C for 5 min. Cells were fixed and permeabilized in 70% (v/v) methanol and 30% (v/v) acetone overnight, blocked with 3% (w/v) BSA in PBST (1× PBS, 0.1% (v/v) Tween-20, 0.1% (v/v) Triton X-100) for 15 min, and probed for 40 min with rat monoclonal anti-BrdU antibody BU1/75 (ICR1) (Abcam ab6326) diluted 1:500 in 3% (v/v) BSA/PBST. Slides were washed thrice in PBST before detection with fluorescein isothiocyanate (FITC)-conjugated goat anti-rat IgG secondary antibody (Jackson ImmunoResearch laboratories) diluted 1:500 in 3% (v/v) BSA/PBST for 20 min. For conjoint detection of ssDNA, p-RPA and degron-RAD51, cells prepared as before for anti-BrdU staining were co-stained with rabbit polyclonal anti–phospho-Thr21–specific RPA32/RPA2 (Abcam ab21551) diluted 1:500, and mouse monoclonal anti-RAD51 antibody 14B4 (Abcam ab213) diluted 1:200. Detection was carried out with AlexaFluor-568 (Invitrogen)–conjugated goat anti-rabbit IgG secondary antibody and AlexaFluor-633 (Invitrogen)–conjugated goat anti-mouse IgG secondary antibody, both diluted 1:500. For anti–cyclin B2 localization, cells were fixed with 4% (v/v) paraformaldehyde for 10 min at room temperature, permeabilized with 0.1% (v/v) TritonX-100 and 0.1% (v/v) Tween-20 for 15 min, blocked for 30 min in 3% (v/v) BSA/PBST, and probed with rabbit polyclonal anti–cyclin B2 antibody[54] diluted at 1:1000. Slides were mounted with Vectashield mounting medium containing 4′,6-diamidino-2-phenylindole (DAPI). Imaging was performed on a Zeiss LSM510 Meta confocal microscope, using a 40× objective with fixed optical slice, laser power and detector/amplifier settings for all samples across each individual experiment to allow comparison.

Automated microscopy. Automated microscopy was performed on an Olympus ScanR high-content screening microscope using a 40× nonimmersion lens. Slides were autofocused using a stepped image-intensity algorithm for the DAPI nuclear signal. Twenty-five 40× fields (~1,000–2,000 DT40 cells) were imaged for each slide with DAPI, FITC and tetramethylrhodamine B isothiocyanate conjugate (TRITC) channels obtained for each position using a triband, dichroic and real-time controlled channel-specific illumination from a MT20 Hg-Xenon light source, with fixed exposure times between samples. The images were stored in the ScanR format for quantitative analysis. DAPI intensity was used to define the nucleus, the 'watershed' function, to separate closely spaced cells, and gating on circularity and area to discard aggregates and incompletely defined cells. Foci were enumerated as secondary objects with a peak pixel intensity algorithm, calibrated using positive and negative controls, by visual inspection of the generated pseudocolor image against the raw grayscale image. The optimized parameters were held constant for analysis of all data sets. The output parameter for each analysis was the number of foci in each channel per cell, with the mean and standard error calculated by the ScanR software. Statistical analyses are described elsewhere.

DNA replication assay. Measurements were performed as previously described[55]. Briefly, genomic DNA was labeled to saturation over 12 h by the incubation of cells with [^{14}C]thymidine (Amersham) at 50 nCi ml^{-1} before extensive washing in PBS. Nascent DNA was labeled with [^{3}H]thymidine (Amersham) at 2 μCi ml^{-1} per 5×10^4 cells for 10 min before harvesting by centrifugation. Cell pellets were washed extensively in PBS and lysed in 0.2 ml 0.25 M NaOH and 6 ml scintillation cocktail (Ultima Gold, Perkin Elmer) before liquid scintillation counting (dual DPM mode). Nascent DNA synthesis was calculated as the ratio of ^{3}H-^{14}C incorporation, thus normalizing it to genomic DNA content.

Statistical analyses. All statistical analyses were performed using GraphPad Prism version 5.00 for Windows, GraphPadSoftware (http://www.graphpad.com).

Comet assays. Comet assays were performed with the CometAssay (Trevigen) kit, in accordance with the manufacturers' instructions.

Note: Supplementary information is available on the Nature Structural & Molecular Biology website.

ACKNOWLEDGMENTS

We are grateful to E. Nigg (Max Planck Institute, Martinsreid, Germany) for providing anti–cyclin B, K. Labib (PICR, Manchester) for providing *pKL187* and S. Takeda (Kyoto University, Japan) for providing the *Rad51*$^{-/-(tetRAD51)}$ DT40 strain. We thank N. Ayoub for help in establishing the degron-EGFP system in DT40, E. Rajendra for technical help with the DT40 experiments and critical review of the manuscript, and members of our laboratory for helpful discussions. X.S. is supported by a studentship from A*STAR, Singapore, and J.A.B. by a

Wellcome Trust grant to A.R.V. Work in A.R.V.'s laboratory is supported by the UK Medical Research Council.

AUTHOR CONTRIBUTIONS

X.S. and J.A.B. together performed the experiments, with J.A.B. as the primary contributor to **Figures 4c** and **5c** and **Supplementary Figure 3**, and X.S. as the primary contributor to the remaining figures. J.A.B. was instrumental in optimizing the experimental conditions for the use of N-end degrons in DT40 cells and provided guidance to X.S. X.S., J.A.B. and A.R.V. interpreted the data. X.S. and J.A.B. prepared the figures. A.R.V. supervised the work and wrote the paper with the help of X.S. and J.A.B.

Published online at http://www.nature.com/nsmb/
Reprints and permissions information is available online at http://npg.nature.com/reprintsandpermissions/

1. Paques, F. & Haber, J.E. Multiple pathways of recombination induced by double-strand breaks in *Saccharomyces cerevisiae*. *Microbiol. Mol. Biol. Rev.* **63**, 349–404 (1999).
2. West, S.C. Molecular views of recombination proteins and their control. *Nat. Rev. Mol. Cell Biol.* **4**, 435–445 (2003).
3. Hoeijmakers, J.H. Genome maintenance mechanisms for preventing cancer. *Nature* **411**, 366–374 (2001).
4. Wang, X. & Haber, J.E. Role of *Saccharomyces* single-stranded DNA-binding protein RPA in the strand invasion step of double-strand break repair. *PLoS Biol.* **2**, e21 (2004).
5. Sugawara, N., Wang, X. & Haber, J.E. *In vivo* roles of Rad52, Rad54, and Rad55 proteins in Rad51-mediated recombination. *Mol. Cell* **12**, 209–219 (2003).
6. Kanaar, R., Hoeijmakers, J.H. & van Gent, D.C. Molecular mechanisms of DNA double strand break repair. *Trends Cell Biol.* **8**, 483–489 (1998).
7. Sung, P., Krejci, L., Van Komen, S. & Sehorn, M.G. Rad51 recombinase and recombination mediators. *J. Biol. Chem.* **278**, 42729–42732 (2003).
8. Wyman, C., Ristic, D. & Kanaar, R. Homologous recombination-mediated double-strand break repair. *DNA Repair (Amst.)* **3**, 827–833 (2004).
9. Symington, L.S. Role of RAD52 epistasis group genes in homologous recombination and double-strand break repair. *Microbiol. Mol. Biol. Rev.* **66**, 630–670 (2002).
10. Sonoda, E. *et al.* Rad51-deficient vertebrate cells accumulate chromosomal breaks prior to cell death. *EMBO J.* **17**, 598–608 (1998).
11. Takata, M. *et al.* The Rad51 paralog Rad51B promotes homologous recombinational repair. *Mol. Cell. Biol.* **20**, 6476–6482 (2000).
12. Takata, M. *et al.* Chromosome instability and defective recombinational repair in knockout mutants of the five Rad51 paralogs. *Mol. Cell. Biol.* **21**, 2858–2866 (2001).
13. Patel, K.J. *et al.* Involvement of Brca2 in DNA repair. *Mol. Cell* **1**, 347–357 (1998).
14. Eppink, B., Wyman, C. & Kanaar, R. Multiple interlinked mechanisms to circumvent DNA replication roadblocks. *Exp. Cell Res.* **312**, 2660–2665 (2006).
15. Dronkert, M.L. & Kanaar, R. Repair of DNA interstrand cross-links. *Mutat. Res.* **486**, 217–247 (2001).
16. Patel, K.J. & Joenje, H. Fanconi anemia and DNA replication repair. *DNA Repair (Amst.)* **6**, 885–890 (2007).
17. Lomonosov, M., Anand, S., Sangrithi, M., Davies, R. & Venkitaraman, A.R. Stabilization of stalled DNA replication forks by the BRCA2 breast cancer susceptibility protein. *Genes Dev.* **17**, 3017–3022 (2003).
18. Henry-Mowatt, J. *et al.* XRCC3 and Rad51 modulate replication fork progression on damaged vertebrate chromosomes. *Mol. Cell* **11**, 1109–1117 (2003).
19. Lusetti, S.L. & Cox, M.M. The bacterial RecA protein and the recombinational DNA repair of stalled replication forks. *Annu. Rev. Biochem.* **71**, 71–100 (2002).
20. Khakhar, R.R., Cobb, J.A., Bjergbaek, L., Hickson, I.D. & Gasser, S.M. RecQ helicases: multiple roles in genome maintenance. *Trends Cell Biol.* **13**, 493–501 (2003).
21. Michel, B., Grompone, G., Flores, M.J. & Bidnenko, V. Multiple pathways process stalled replication forks. *Proc. Natl. Acad. Sci. USA* **101**, 12783–12788 (2004).
22. Yu, V.P. *et al.* Gross chromosomal rearrangements and genetic exchange between nonhomologous chromosomes following BRCA2 inactivation. *Genes Dev.* **14**, 1400–1406 (2000).
23. Dohmen, R.J., Wu, P. & Varshavsky, A. Heat-inducible degron: a method for constructing temperature-sensitive mutants. *Science* **263**, 1273–1276 (1994).
24. Bachmair, A., Finley, D. & Varshavsky, A. *In vivo* half-life of a protein is a function of its amino-terminal residue. *Science* **234**, 179–186 (1986).
25. Labib, K., Tercero, J.A. & Diffley, J.F. Uninterrupted MCM2–7 function required for DNA replication fork progression. *Science* **288**, 1643–1647 (2000).
26. Fukagawa, T., Regnier, V. & Ikemura, T. Creation and characterization of temperature-sensitive CENP-C mutants in vertebrate cells. *Nucleic Acids Res.* **29**, 3796–3803 (2001).
27. Sonoda, E. *et al.* Sister chromatid exchanges are mediated by homologous recombination in vertebrate cells. *Mol. Cell. Biol.* **19**, 5166–5169 (1999).
28. Dodson, H. *et al.* Centrosome amplification induces by DNA damage occurs during a prolonged G2 phase and involves ATM. *EMBO J.* **23**, 3864–3873 (2004).
29. Zou, L. & Elledge, S.J. Sensing DNA damage through ATRIP recognition of RPA-ssDNA complexes. *Science* **300**, 1542–1548 (2003).
30. Block, W.D., Yu, Y. & Lees-Miller, S.P. Phosphatidyl inositol 3-kinase-like serine/threonine protein kinases (PIKKs) are required for DNA damage-induced phosphorylation of the 32 kDa subunit of replication protein A at threonine 21. *Nucleic Acids Res.* **32**, 997–1005 (2004).
31. Raderschall, E., Golub, E.I. & Haaf, T. Nuclear foci of mammalian recombination proteins are located at single-stranded DNA regions formed after DNA damage. *Proc. Natl. Acad. Sci. USA* **96**, 1921–1926 (1999).
32. Savage, J.R. Classification and relationships of induced chromosomal structural changes. *J. Med. Genet.* **13**, 103–122 (1976).
33. Haber, J.E. DNA recombination: the replication connection. *Trends Biochem. Sci.* **24**, 271–275 (1999).
34. Aguilera, A. & Gomez-Gonzalez, B. Genome instability: a mechanistic view of its causes and consequences. *Nat. Rev. Genet.* **9**, 204–217 (2008).
35. Michel, B. *et al.* Rescue of arrested replication forks by homologous recombination. *Proc. Natl. Acad. Sci. USA* **98**, 8181–8188 (2001).
36. Kogoma, T. Recombination by replication. *Cell* **85**, 625–627 (1996).
37. Kuzminov, A. Collapse and repair of replication forks in *Escherichia coli*. *Mol. Microbiol.* **16**, 373–384 (1995).
38. Merrill, B.J. & Holm, C. The RAD52 recombinational repair pathway is essential in pol30 (PCNA) mutants that accumulate small single-stranded DNA fragments during DNA synthesis. *Genetics* **148**, 611–624 (1998).
39. Tsuzuki, T. *et al.* Targeted disruption of the Rad51 gene leads to lethality in embryonic mice. *Proc. Natl. Acad. Sci. USA* **93**, 6236–6240 (1996).
40. Shinohara, A., Ogawa, H. & Ogawa, T. Rad51 protein involved in repair and recombination in *S. cerevisiae* is a RecA-like protein. *Cell* **69**, 457–470 (1992).
41. Muris, D.F. *et al.* Homologous recombination in the fission yeast *Schizosaccharomyces pombe*: different requirements for the *rhp51*+, *rhp54*+ and *rad22*+ genes. *Curr. Genet.* **31**, 248–254 (1997).
42. Lopes, M., Foiani, M. & Sogo, J.M. Multiple mechanisms control chromosome integrity after replication fork uncoupling and restart at irreparable UV lesions. *Mol. Cell* **21**, 15–27 (2006).
43. Mojas, N., Lopes, M. & Jiricny, J. Mismatch repair-dependent processing of methylation damage gives rise to persistent single-stranded gaps in newly replicated DNA. *Genes Dev.* **21**, 3342–3355 (2007).
44. Stojic, L. *et al.* Mismatch repair-dependent G2 checkpoint induced by low doses of SN1 type methylating agents requires the ATR kinase. *Genes Dev.* **18**, 1331–1344 (2004).
45. Sogo, J.M., Lopes, M. & Foiani, M. Fork reversal and ssDNA accumulation at stalled replication forks owing to checkpoint defects. *Science* **297**, 599–602 (2002).
46. Lopes, M. *et al.* The DNA replication checkpoint response stabilizes stalled replication forks. *Nature* **412**, 557–561 (2001).
47. Meister, P. *et al.* Temporal separation of replication and recombination requires the intra-S checkpoint. *J. Cell Biol.* **168**, 537–544 (2005).
48. Liberi, G. *et al.* Rad51-dependent DNA structures accumulate at damaged replication forks in *sgs1* mutants defective in the yeast ortholog of BLM RecQ helicase. *Genes Dev.* **19**, 339–350 (2005).
49. Branzei, D. *et al.* Ubc9- and mms21-mediated sumoylation counteracts recombinogenic events at damaged replication forks. *Cell* **127**, 509–522 (2006).
50. Pfander, B., Moldovan, G.L., Sacher, M., Hoege, C. & Jentsch, S. SUMO-modified PCNA recruits Srs2 to prevent recombination during S phase. *Nature* **436**, 428–433 (2005).
51. Sanchez-Diaz, A., Kanemaki, M., Marchesi, V. & Labib, K. Rapid depletion of budding yeast proteins by fusion to a heat-inducible degron. *Sci. STKE* **223**, pl8 (2004).
52. Yu, D.S. *et al.* Dynamic control of Rad51 recombinase by self-association and interaction with BRCA2. *Mol. Cell* **12**, 1029–1041 (2003).
53. Niedzwiedz, W. *et al.* The Fanconi anaemia gene FANCC promotes homologous recombination and error-prone DNA repair. *Mol. Cell* **15**, 607–620 (2004).
54. Gallant, P. & Nigg, E.A. Cyclin B2 undergoes cell cycle-dependent nuclear translocation and, when expressed as a non-destructible mutant, causes mitotic arrest in HeLa cells. *J. Cell Biol.* **117**, 213–224 (1992).
55. Sangrithi, M.N. *et al.* Initiation of DNA replication requires the RECQL4 protein mutated in Rothmund-Thomson syndrome. *Cell* **121**, 887–898 (2005).
56. Sonoda, E. *et al.* Scc1/Rad21/Mcd1 is required for sister chromatid cohesion and kinetochore function in vertebrate cells. *Dev. Cell* **1**, 759–770 (2001).